Intermode dephasing in a superconducting stripline resonator

Oren Suchoi,[1] Baleegh Abdo,[1] Eran Segev,[1] Oleg Shtempluck,[1] M. P. Blencowe,[2] and Eyal Buks[1]

[1]*Department of Electrical Engineering, Technion, Haifa 32000, Israel*
[2]*Department of Physics and Astronomy, Dartmouth College, Hanover, New Hampshire 03755, USA*

We study a superconducting stripline resonator (SSR) made of niobium, which is integrated with a superconducting interference device (SQUID). The large nonlinear inductance of the SQUID gives rise to a strong Kerr nonlinearity in the response of the SSR, which in turn results in strong coupling between different modes of the SSR. We experimentally demonstrate that such intermode coupling gives rise to dephasing of microwave photons. The dephasing rate depends periodically on the external magnetic flux applied to the SQUID, where the largest rate is obtained at half integer values (in units of the flux quantum). To account for our result we compare our findings with theory and find good agreement.

I. INTRODUCTION

Dephasing is the suppression process of quantum coherent effects due to coupling between a quantum system and its external environment.[1] A Kerr nonlinearity in an electromagnetic resonator may lead to dispersive intermode coupling, which in turn may result in dephasing of photons.[2,3] Such a coupling mechanism can also be exploited to allow quantum nondemolition (QND) detection of single photons.[2,4–7] A Kerr nonlinearity exists in superconducting stripline resonators (SSR) due to the effect of kinetic inductance. However, the resultant intermode coupling is typically far too weak to allow any significant dephasing.[8] On the other hand, a much stronger Kerr nonlinearity can be achieved by integrating a superconducting interference device (SQUID) with the SSR.[9–11] External magnetic flux can be employed in these devices to modulate both the linear and nonlinear contributions to the inductance of the SQUID, which in turn allows external control of both the resonance frequencies and the strength of Kerr nonlinearity, respectively. The enhanced Kerr nonlinearity also provides strong coupling between different modes in the resonator that causes dephasing of one mode (called the *system* mode) when another one (the *detector* mode) is externally driven at relatively high powers.

Here, we employ such a configuration consisting of a Niobium SSR and incorporating a SQUID device having a nanobridge in each of its two arms. We monitor the resonance lineshape of one of the modes of the resonator (the *system* mode) as we simultaneously drive another one (the *detector* mode). We find that a significant broadening of the resonance lineshape of the system mode occurs in the same region where the response of the detector mode, which is measured simultaneously, becomes strongly nonlinear. We provide theoretical evidence to substantiate our hypothesis that the underlying mechanism responsible for the observed broadening is intermode dephasing. The ability to externally control the strength of the intermode coupling, which in turn controls the dephasing rate, makes our device an ideal tool for experimentally studying fundamental issues related to the quantum-classical transition.[1] Moreover, dephasing process is important in quantum limited measurement which requires that the dephasing time of a superposition of two states due

to the measurement process be the same as the lifetime of the superposition.[12–14]

II. EXPERIMENTAL SYSTEM

Figure 1 schematically shows the device. The SSR (Refs. 11, 15, and 16) comprises two identical stripline sections connected by a SQUID. A nanobridge[17–20] on each arm of the SQUID loop serves as a weak link. The critical currents of the nanobridges are denoted by I_{c1} and I_{c2}, respectively. Both nanobridges are assumed to have the same capacitance C_J. The self inductance of the loop is denoted by Λ. A feedline, which is weakly coupled to the SSR, is employed to deliver the input and output microwave signals. The experimental setup is presented in subplot (a) of Fig. 1.

The fabrication process starts with a high-resistivity Si substrate coated with SiN layers of thickness of 100 nm on both sides. A 150 nm thick Nb layer is deposited on the wafer using magnetron dc sputtering. Then, e-beam lithography and a subsequent lift-off process are employed to pattern an Al mask, which defines the SSR and the SQUID leads. The device is then etched using electron cyclotron resonance system with CF_4 plasma. The nanobridges are fabricated using FEI Strata 400 focus ion beam (FIB) system[21–25] at accelerating voltage of 30 kV and Ga ions current of 9.7 pA. The outer dimensions of the bridges are about 150×50 nm. However, the actual dimensions of the weak links are smaller since the bombarding Ga ions penetrate into the Nb layer, and consequently, suppress superconductivity over a depth estimated between 30 and 50 nm.[25,26]

III. EFFECTIVE HAMILTONIAN

The effective Hamiltonian of the closed system consisting of the SSR and the SQUID, expressed in terms of the annihilation and creation operators A_1, $A_1^\dagger$, A_3, and $A_3^\dagger$ of the first and third modes respectively, is given by

$$\mathcal{H}_{\text{eff}} = \hbar\omega_1 N_1 + \hbar\omega_3 N_3 + V_{\text{in}} + \hbar K_1 N_1^2 + \hbar\lambda_{1,3} N_1 N_3, \quad (1)$$

where $N_1 = A_1^\dagger A_1$ and $N_3 = A_3^\dagger A_3$ are number operators, $V_{\text{in}} = \hbar\sqrt{2\gamma_{\text{f1}}} b_1^{\text{in}}(e^{-i\omega_p t} A_1 + e^{i\omega_p t} A_1^\dagger)$ represents the external driving, γ_{f1} is the coupling constant between the first mode and the
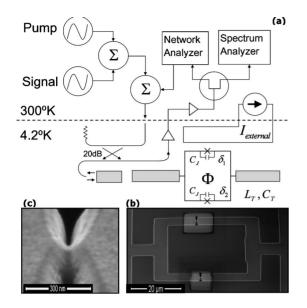
FIG. 1. (a) The device and the experimental setup. The SSR is made of two identical stripline sections of length $l_T/2=110$ mm, each having inductance L_T and capacitance C_T per unit length and characteristic impedance $Z_T=\sqrt{L_T/C_T}=50$ Ω. The stripline sections are connected by a SQUID consisting of nanobridge type weak links. All measurements are done at liquid Helium temperature 4.2 K, where the device is placed inside a copper package, which is internally coated with Nb (to reduce surface resistance and to provide magnetic shielding). (b) SEM micrograph of the SQUID (tilted view). The loop area is 39×39 μm^2. (c) SEM micrograph of the nanobridge.

feedline, b_1^{in} is the amplitude of the driving pump tone which is injected into the feedline to excite the first mode, and where ω_p is its angular frequency. The full Derivation of the Hamiltonian is given in Appendix A. The last two terms represent the Kerr nonlinearity term of the first, externally driven (detector) mode and the intermode coupling between the first and the third (system) modes, respectively. The coefficients ω_1, ω_3, K_1, and $\lambda_{1,3}$, which are calculated in Appendix A, depend periodically on the external flux Φ_x with period Φ_0. The flux dependence of ω_1 and ω_3 can be attributed to the inductance of the SQUID, which is proportional to the second derivative of ε_0 with respect to I, where ε_0 is the ground state energy of the SQUID. On the other hand, both the Kerr nonlinearity K_1 and intermode coupling $\lambda_{1,3}$ coefficients are proportional to the nonlinear inductance of the SQUID,[27] which in turn is proportional to the fourth derivative of ε_0 with respect to I.

The use of nanobridge based SQUIDs instead of Al/Al$_2$O$_3$/Al junctions was preferred due to the low capacitance of the nanobridge junctions, which allows us to use the adiabatic approximation in the derivation of the Hamiltonian. Recently, we have published results[28] obtained from a similar configuration using a dc-SQUID with Al/Al$_2$O$_3$/Al junctions that showed large parametric gain but did not show the intermode coupling effects that are the subject of this article.

IV. RESONANCE FREQUENCY SHIFT

Figure 2 shows measurements of the reflection coefficient $|S_{11}|$ (S_{11} is the ratio between the reflected outgoing and the
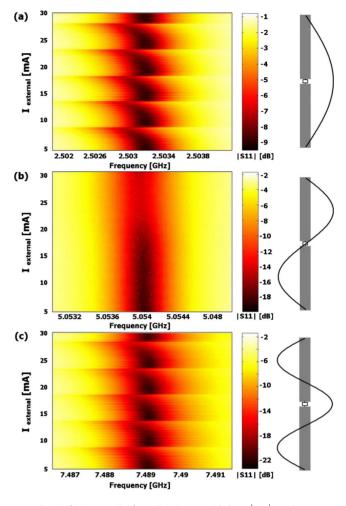

FIG. 2. (Color online) Reflection coefficient $|S_{11}|$ vs frequency and external flux for the first 3 modes of the SSR. A change of 4.8 mA in the external current corresponds to a change of Φ_0 in the magnetic flux.

injected incoming amplitudes in the feedline) of the first three modes of the resonator as a function of frequency and externally applied flux Φ_x. The sketches on the right hand side show the current waveform of each mode. For the first and the third modes, S_{11} is found to be a periodic function of Φ_x with period Φ_0, where $\Phi_0=h/2e$ is the flux quantum. On the other hand, the second mode, which is decoupled from the SQUID since its current waveform has a node at the location of the SQUID, does not exhibit a flux dependence. Note that the data in Fig. 2 is obtained by sweeping the magnetic flux upwards. However, as can be seen from Fig. 3(a), in which the resonance frequency $f_1=\omega_1/2\pi$ of the first mode is measured versus both increasing (blue) and decreasing (red) magnetic flux, the response is hysteretic.

The solid black line in Fig. 3(a) is obtained by numerically evaluating the resonance frequency $f_1=\omega_1/2\pi$ using Eq. (8) in Appendix A. For the parameters that are used in the calculation for this case (see figure caption), the SQUID can be either monostable or bistable depending on Φ_x. Consequently, sharp transitions occur near the values of Φ_x corresponding to a boundary between these regions, and as a result, the response is hysteretic. Interestingly, as the input
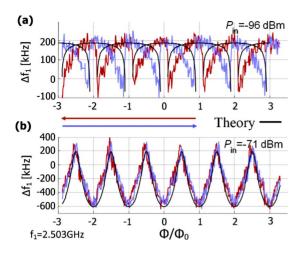
FIG. 3. (Color online) The resonance frequency shift Δf_1 of the first (detector) mode vs. applied flux for two different values of P_{in}. The flux is first swept upwards (blue line) and than downwards (red line). The black solid lines represent the theoretical calculation of Δf_1 using the following parameters: $\beta_L = 7.4$ for $P_{in} = -96$ dBm, $\beta_L = 0.15$ for $P_{in} = -71$ dBm, and $I_{c1}/I_{c2} = 3$ for both cases.

power is increased the response becomes nonhysteretic, as can be seen from Fig. 3(b), which shows a measurement of f_1 at $P_{in} = -71$ dBm. Theoretically, this behavior is accounted for by assuming that the value of the screening parameter $\beta_L = 2\pi\Lambda I_c/\Phi_0$, which is proportional to the average critical current $I_c = (I_{c1} + I_{c2})/2$, is significantly lower for this case (0.15 instead of the value 7.4, which was used to fit the data for $P_{in} = -96$ dBm). To account for this behavior we discuss in Appendix B the possibility that local heating of the

nanobridges is responsible for the drop in I_c at elevated input powers. Assuming that the heat is mainly dissipated down into the substrate rather than along the film, we estimate that the temperature rise for $P_{in} = -70$ dBm is 4 K. This rough estimation indicates that heating may indeed play an important role, and may be held responsible for the apparent drop in the critical current.

V. INTERMODULATION AND INTERMODE DEPHASING

Both nonlinear terms in the Hamiltonian $\mathcal{H}_{eff}$ (1) play an important role as P_{in} is increased. The effect of the Kerr nonlinearity can be sensitively observed by employing intermodulation (IM) characterization.[27] In this method, in addition to the relatively strong *pump* tone at frequency ω_p, which is used to drive the first mode to any desirable operating point, another tone, called *signal*, which has a much smaller power $P_{s,in}$ and a nearby frequency $\omega_p + \delta\omega$ ($\delta\omega$ is much smaller than the resonance width), is also injected simultaneously into the feedline. Due to Kerr nonlinearity these two inputs may mix in the resonator and produce tones of IM products. Typically, the largest IM products are the output signal at frequency $\omega_p + \delta\omega$ and the output idler at frequency $\omega_p - \delta\omega$. The two corresponding gain factors, namely the signal gain $G_s = P_{s,out}/P_{s,in}$ and the idler gain $G_i = P_{i,out}/P_{s,in}$, where $P_{s,out}$ and $P_{i,out}$ are the powers of the output signal and output idler tones respectively, were evaluated in Ref. 27. Panel (b) of Fig. 4 presents a color map showing IM characterization of the first (detector) mode, which was obtained using a spectrum analyzer. The powers of the injected pump and signal tones in the IM measurement
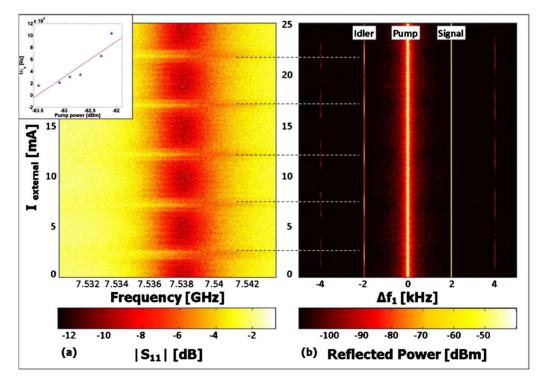

FIG. 4. (Color online) IM characterization of the detector mode [panel (b)] and $|S_{11}|$ measurements of the system mode [panel (a)]. Largest idler gain as well as highest dephasing rate is obtained at half integer values of the externally applied flux. The pump frequency is $\omega_p = \omega_1(\Phi = 0)$. The inset shows the dephasing rate as a function of the pump power.
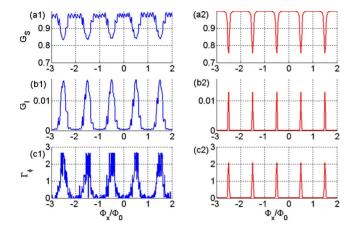
FIG. 5. (Color online) Signal gain G_s, idler gain G_i, and normalized dephasing rate Γ_φ. Experimental results are shown in panels (a1), (b1), and (c1), whereas theoretical predictions are shown in panels (a2), (b2), and (c2). The following device parameters were taken in order to evaluate G_s and G_i theoretically using Eqs. (82) and (83) of Ref. 27 [panels (a2) and (b2) respectively)], and to evaluate Γ_φ using Eq. (70) of Ref. 8 [panel (c2)]: $(\gamma_{f3} + \gamma_{d3})/\omega_1$ =5000, γ_{f3}/γ_{d3}=0.15, I_{c1}=1.5 μA, and I_{c2}=4.5 μA. Note that the effect of nonlinear damping (Ref. 27) is disregarded.

are −62.1 and −81 dBm, respectively. The pump power was chosen to be large enough so that the SQUID is monostable for all flux values. Both G_s and G_i periodically oscillate as a function of the external current. This behavior is seen more clearly in panels (a1) and (b1) of Fig. 5 which exhibit G_s and G_i versus Φ_x/Φ_0.

The intermode coupling term in Hamiltonian (1) can be exploited to continuously measure the number of photons in the system mode by externally driving the detector mode.[2,3] Such a measurement scheme is characterized by the time it takes to resolve adjacent number states of the system mode. Significant dephasing occurs when this time scale is made comparable or shorter than the lifetime of photons in the system mode. Theoretically, dephasing of photons in the system mode is expected to give rise to a resonance frequency shift and to broadening of the resonance line shape of the power reflection coefficient $|S_{11}(\omega)|^2$, which is given by[29]

$$|S_{11}(\omega)|^2 = 1 - \frac{\gamma_{f3}\gamma_{d3}}{\gamma_{f3} + \gamma_{d3}} \frac{4\gamma_{\text{tot}}}{\gamma_{\text{tot}}^2 + (\omega - \tilde{\omega}_3)^2}, \qquad (2)$$

where $\tilde{\omega}_3$ is the shifted angular resonance frequency, the total width is given by $\gamma_{\text{tot}} = \gamma_{f3} + \gamma_{d3} + 1/\tau_\varphi$, where γ_{f3} denotes the coupling constant between the system mode and the feedline, γ_{d3} denotes the damping rate of the system mode and $1/\tau_\phi$ is the dephasing rate of photons in the system mode.

Simultaneously with the IM characterization, we also measure the resonance line shape of the third mode using a network analyzer. A very low-input power of −101 dBm is employed to avoid any nonlinear response of the third mode. As can be seen from the results, which are presented in panel (a) of Fig. 4, the measured reflection coefficient $|S_{11}(\omega)|^2$ periodically oscillates as a function of Φ_x. Fitting the experimental data to Eq. (2) yields the normalized dephasing rate $\Gamma_\varphi = 1/(\gamma_{f3} + \gamma_{d3})\tau_\varphi$. As can be seen from Fig. 5, at the same

points where G_i peaks [panel (b1)], namely for half integer values of the external flux, a strong peak is found in Γ_φ [panel (c1)]. At these points, the value of Γ_φ exceeds unity, namely, the dephasing rate becomes larger than the system mode decay rate. The inset in Fig. 4 shows the increase in the dephasing rate as the pump power is increased.

To account for the experimental results, we employ Eqs. (82) and (83) of Ref. 27 to calculate the gain factors G_s and G_i, respectively, and Eq. (70) of Ref. 8 to calculate the normalized dephasing rate Γ_φ. Note that weak nonlinearity approximation is employed in these calculations, namely, nonlinearity is taken into account only to lowest nonvanishing order. The results, given in panels (a2), (b2), and (c2) of Fig. 5 yield fairly good agreement with the experimental data [panels (a1), (b1), and (c1)]. The device parameters that were used in the calculation are listed in the figure caption. The flux dependence of the gain factors G_s and G_i and that of the normalized dephasing rate Γ_φ can be attributed to the periodic flux dependence of the parameters ω_1, ω_3, K_1, and $\lambda_{1,3}$ of Hamiltonian (1). Both nonlinear parameters K_1 and $\lambda_{1,3}$ peak at half integer values of the external flux. Consequently, both G_i, which can be considered as a measure of the strength of nonlinearity, and Γ_φ, which strongly depends on $\lambda_{1,3}$, obtain their largest values at these points.

VI. RESONANCE BROADENING DUE TO SHUNT RESISTANCE

In principle, the effect of resonance lineshape variation with magnetic flux can alternatively be explained by taking into account the effect of quasiparticles in the junctions that provide shunting resistance. To estimate the contribution of this possibly competing effect, we treat the dc-SQUID as a flux dependent inductor having inductance L_S, connected in parallel with a shunt resistor R_J. Assuming $L_S/L_T l_T \ll 1$ (see Appendix A) and employing the expressions derived in Ref. 30 for the resonance frequency ω_T (generalized for the present case, where the impedance of the dc-SQUID has nonvanishing real part due to the shunt resistance), we find that ω_T becomes complex

$$\omega_T = \frac{\pi}{l_T\sqrt{L_T C_T}}\left[1 + \frac{L_S}{L_T l_T}\frac{1 - \dfrac{2i\omega_p L_S}{R_J}}{1 + \left(\dfrac{2\omega_p L_S}{R_J}\right)^2}\right]. \qquad (3)$$

While the real part of ω_T is the flux-dependent angular resonance frequency, the imaginary part is the contribution $\Delta\gamma$ to the damping rate due to the shunt resistance. Based on the parameters of our device we estimate that the ratio $\Delta\gamma/\Delta\omega$ is less than 0.02, where $\Delta\omega$ is the flux induced shift in the resonance frequency. On the other hand, the data demonstrates values of the ratio $\Delta\gamma/\Delta\omega$ that exceed 20. Thus, we conclude that this effect cannot fully account for the results presented above.

VII. CONCLUSION

Integrating a SQUID having large nonlinear inductance with an SSR leads to strong IM distortion and strong inter-

mode coupling. In the present paper, we have exploited these effects to study a novel mechanism of dephasing of microwave photons that can be externally controlled. The same intermode coupling that is responsible for the observed photon dephasing can also be exploited for single photon detection.[2,3] In future experiments several improvements, such as increasing the nonlinear coupling, as well as reducing the temperature and using lower noise preamplifier should allow detection of single microwave photons.

APPENDIX A: DETAILED DERIVATION OF THE EFFECTIVE HAMILTONIAN

The effective Hamiltonian of the closed system comprising the SSR and the SQUID (Refs. [15] and [31]) is found using the same method that was previously employed in Refs. [16] and [31]. Here, however, we relax the assumption that the self inductance of the SQUID loop is small, and also the assumption that both junctions have the same critical currents. On the other hand, we assume that the inductance of the SQUID, which is denoted as L_S, is much smaller than the total inductance of the stripline $L_T l_T$. This assumption can be justified by considering the fact that the measured angular resonance frequencies ω_n of the first three modes ($n \in \{1,2,3\}$) for all values of Φ_x (see Figs. [2] and [3] in the paper body) are very close to the values expected from a uniform resonator having length l_T, namely, $n\omega_T$, where $\omega_T = \pi/l_T\sqrt{L_T C_T}$. Moreover, the normalized flux-induced shift $\Delta\omega_n/n\omega_T$ in the angular resonance frequency of the first three modes is quite small and never exceeds 10^{-3}. Both observations indicate that the ratio $L_S/L_T l_T$ can indeed be considered as a small parameter.

The resultant Hamiltonian of the closed system is given by $\mathcal{H} = \mathcal{H}_{\text{SSR}} + \mathcal{H}_S(I)$, where $\mathcal{H}_{\text{SSR}}$ is the SSR Hamiltonian and where $\mathcal{H}_S(I)$ is the SQUID Hamiltonian, which depends on the current I at the center of the SSR, namely, the current flowing through the SQUID. In terms of annihilation (A_1 and A_3) and creation ($A_1^\dagger$ and $A_3^\dagger$) operators for the first and third modes of the SSR, respectively, the Hamiltonian $\mathcal{H}_{\text{SSR}}$ can be expressed as

$$\mathcal{H}_{\text{SSR}} = \hbar\omega_T(N_1 + 3N_3) + V_{\text{in}}, \tag{4}$$

where $N_1 = A_1^\dagger A_1$ and $N_3 = A_3^\dagger A_3$ are number operators,

$$V_{\text{in}} = \hbar\sqrt{2\gamma_{\text{f1}}}\, b_1^{\text{in}}(e^{-i\omega_p t}A_1 + e^{i\omega_p t}A_1^\dagger) \tag{5}$$

represents the external driving, γ_{f1} is the coupling constant between the first mode and the feedline, b_1^{in} is the amplitude of the driving pump tone, which is injected into the feedline to excite the first mode, and ω_p is its angular frequency.

1. Kinetic inductance of the nanobridges

The Hamiltonian for the SQUID depends on the properties of the nanobridges. Due to the Ga ions implanted in the outer layer of the Niobium during the FIB process and the consequent suppression of superconductivity in that layer,[25,26] the weak links are treated as variable thickness nanobridges. The behavior of such a nanobridge is strongly dependent on the ratio l/ξ,[17,20,32–37] where l is the bridge length and ξ is the coherence length of the Cooper pairs. The coherence length ξ depends also on the temperature of the bridge. In the dirty limit ξ is given by $\xi(T) = 0.852\sqrt{\xi_0 l_f (T_C/T - 1)^{-1}}$,[17] where ξ_0 is the size of the cooper pair and l_f is the mean free path.[38,39] The current-phase relation (CPR) of the bridges is periodic with respect to the gauge invariant phase δ across the bridge. When $l/\xi(T) \ll 1$, the nanobridge behaves like a regular Josephson junction (JJ) with a sinusoidal CPR.[40] However, as the ratio $l/\xi(T)$ becomes larger, the CPR deviates from the sinosoidal form and can also become multivalued.[17] In case the CPR is not multivalued the bridge can be approximately considered as a JJ having an extra kinetic inductance L_K. The effect of the kinetic inductance can be taken into account by replacing the screening parameter of the loop $\beta_L = 2\pi\Lambda I_c/\Phi_0$ by an effective one given by $\beta_L + \Delta\beta$, where $\Delta\beta = 2\pi L_K I_c/\Phi_0$.

In order to estimate $\Delta\beta$ we use Eqs. (47)–(49) and the data in Fig. 5 of Ref. [18]. For $l/\xi = 1.7$ the bridges' contribution is $\Delta\beta \simeq 1$. As we will discuss below, both β_L and $\Delta\beta$ depend on the injected power P_{in} that is used to excite the resonator due to a heating effect. However, for all values of P_{in} that were used in our experiment, we estimate that the ratio $\Delta\beta/\beta_L$ never exceeds the value of 0.5 and thus the effect of kinetic inductance can be considered as small. Furthermore, the CPR remains a single valued function in the entire range of parameters that is explored in our experiments. Consequently, the nanobridges can be treated as regular JJs to a good approximation.

2. SQUID Hamiltonian

In the following derivation we treat the nanobridges as regular JJs. We consider the case where the critical currents of both nanobridges are $I_{c1} = I_c(1+\alpha)$ and $I_{c2} = I_c(1-\alpha)$, respectively, where the dimensionless parameter α characterizes the asymmetry in the SQUID. The Hamiltonian for the SQUID, which is expressed in terms of the two gauge invariant phases δ_1 and δ_2 across both junctions, and their canonical conjugates p_1 and p_2, is given by

$$\mathcal{H}_S(I) = \frac{2\pi\omega_p^2(p_1^2 + p_2^2)}{E_0} + E_0 u(\delta_1, \delta_2; I), \tag{6}$$

where $\omega_{pl} = \sqrt{I_c/C_J\Phi_0}$ is the plasma frequency, $E_0 = \Phi_0 I_c/\pi$ is the Josephson energy, and the dimensionless potential u is given by[41]

$$u = -\frac{(1+\alpha)\cos\delta_1 + (1-\alpha)\cos\delta_2}{2} + \frac{\left(\dfrac{\delta_1 - \delta_2}{2} + \dfrac{\pi\Phi_x}{\Phi_0}\right)^2}{\beta_L}$$
$$- \frac{(\delta_1 + \delta_2)I}{4I_c} - \frac{\zeta(\delta_1 + \delta_2)^2}{16}, \tag{7}$$
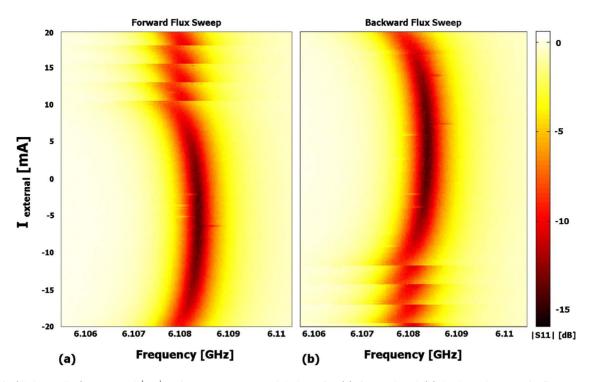
where $\zeta = \Phi_0/2I_c L_T l_T$.

FIG. 6. (Color online) Measured $|S_{11}|$ at input power $P_{\text{in}}=-95$ dBm for (a) forward and (b) backward magnetic flux sweep. In this sample $\beta_L=20$, and the response is highly hysteretic.

3. Adiabatic approximation

Due to the extremely small capacitance C_J of both nanobridges,[42] the plasma frequency ω_{pl} of the SQUID is estimated to exceed 1 THz. Thus, the effect of the SQUID on the SSR, which has a much slower dynamics, can be treated using the adiabatic approximation.[6,30] Formally, treating the current I as a parameter (rather than a degree of freedom), the Hamiltonian $\mathcal{H}_S$ can be diagonalized $\mathcal{H}_S|k(I)\rangle = \varepsilon_k(I)|k(I)\rangle$, where $k=0,1,2,\ldots,$ and $\langle k(I)|l(I)\rangle=\delta_{kl}$. To lowest order in the adiabatic expansion the effective Hamiltonian governing the dynamics of the slow degrees of freedom corresponding to the fast part of the system occupying the state $|k(I)\rangle$ is given by $\mathcal{H}_k^A=\mathcal{H}_{\text{SSR}}+\varepsilon_k(I)$.[43,44] Furthermore, in the limit where the thermal energy $k_B T$ is much smaller than the typical energy spacing between different levels of $\mathcal{H}_1(\simeq\hbar\omega_{\text{pl}})$ one can assume that the SQUID remains in its current dependent ground state $|0(I)\rangle$. For most cases this assumption is valid for our experimental parameters. It is important, however, to note that when the externally applied magnetic flux is close to a half-integer value (in units of Φ_0), namely, when $\Phi_x\simeq(n+1/2)\Phi_0$, where n is integer, this approximation may break down. Near these points the potential u may have two different neighboring wells having similar depth. Consequently, near these points, the energy gap between the ground state and the first excited state can become much smaller than $\hbar\omega_{\text{pl}}$. On the other hand, the ratio between the height of the barrier separating the two wells ($\simeq E_0$) and the energy spacing between intrawell states ($\simeq\hbar\omega_{\text{pl}}$) is typically $E_0/\hbar\omega_{\text{pl}}\simeq 100$ for our samples. Since the coupling between states localized in different wells depends exponentially on this ratio, we conclude that to a good approximation the interwell coupling can be neglected.

Moreover, in the same limit where $E_0/\hbar\omega_{\text{pl}}\gg 1$, one can approximate the ground state energy ε_0 by the value of $E_0 u$ at the bottom of the well where the system is localized.

The current I at the center of the SSR can readably be expressed in terms of the annihilation and creation operators A_1, $A_1^\dagger$, A_3, and $A_3^\dagger$. This allows expanding the current dependent ground state energy $\varepsilon_0(I)$ as a power series of these operators. In the rotating wave approximation oscillating terms in such an expansion are neglected since their effect on the dynamics for a time scale much longer than a typical oscillation period is negligibly small. Moreover, constant terms in the Hamiltonian are disregarded since they only give rise to a global phase factor. In the present experiment the 1st SSR mode is externally driven, and we focus on the resultant dephasing induced on the third mode. To that end we include in the effective Hamiltonian of the closed system in addition to the linear terms corresponding to the 1st and 3rd modes, also the Kerr nonlinearity term of the 1st mode, which is externally driven, and also the term representing intermode coupling between the 1st and the 3rd modes [see Eq. (1)].

The angular resonance frequency shift of the first and the third modes, which is given by

$$\frac{\omega_1-\omega_T}{\omega_T}=\frac{\omega_3-3\omega_T}{3\omega_T}=\zeta\frac{\partial^2(\varepsilon_0/E_0)}{\partial(I/I_c)^2}, \tag{8}$$

can be attributed to the inductance of the SQUID, which is proportional to the second derivative of ε_0 with respect to I. On the other hand, the Kerr nonlinearity, which is given by
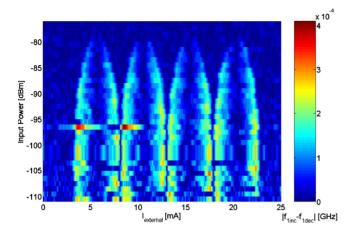
FIG. 7. (Color online) The difference between the measured resonance frequencies obtained in the increasing flux sweep ($f_{1\ inc}$) and the decreasing flux sweep ($f_{1\ dec}$) of the first (*detector*) mode. The dark blue areas correspond to monostable regions, namely, the same resonance frequency is measured for both the increased and decreased sweep. The red indicates the regions where the system is bistable.

$$\frac{K_1}{\omega_1} = \frac{\zeta^2 \hbar \omega_1}{2E_0} \frac{\partial^4(\varepsilon_0/E_0)}{\partial(I/I_c)^4}, \tag{9}$$

and the intermode coupling, which is given by $\lambda_{1,3}=9K_1$, can both be attributed to the nonlinear inductance of the SQUID,[27] which is proportional to the fourth derivative of ε_0 with respect to I.

4. Evaluation of ω_1, ω_3, K_1, and $\lambda_{1,3}$ in the limit $\beta_L \ll 1$

The evaluation of the parameters ω_1, ω_3, K_1, and $\lambda_{1,3}$ generally requires a numerical calculation. However, an analytical approximation can be employed when $\beta_L \ll 1$. In this limit the phase difference $\delta_2 - \delta_1$ is strongly confined near the value $2\pi\Phi_x/\Phi_0$, as can be seen from Eq. (7). This fact can be exploited to further simplify the dynamics by applying another adiabatic approximation, in which the phase difference $\delta_2 - \delta_1$ is treated as a "fast" variable and the phase average $\delta_+ = (\delta_1 + \delta_2)/2$ as a 'slow' one. To lowest order in the adiabatic expansion one finds that for low frequencies $\omega \ll \omega_{pl}$, namely, in the region where the impedance associated with the capacitance of the JJs is much larger in absolute value in comparison with the impedance associated with the inductance, the SQUID behaves as a single JJ having critical current given by[45]

$$I_S = 2I_c \sqrt{1 - (1-\alpha^2)\sin^2(\pi\Phi_x/\Phi_0)}. \tag{10}$$

Note that this approximation may break down when $\Phi_x \simeq (n+1/2)\Phi_0$ unless the asymmetry parameter α is sufficiently large. The relatively large value of α in our device ($\alpha \simeq 0.5$) ensures the validity of the above approximation.

Using this result, it is straightforward to obtain the following analytical approximations:

$$\frac{\partial^2(\varepsilon_0/E_0)}{\partial(I/I_c)^2} = \frac{I_c}{\pi I_S}, \tag{11a}$$

$$\frac{\partial^4(\varepsilon_0/E_0)}{\partial(I/I_c)^4} = -\frac{8}{3\pi^2}\left(\frac{I_c}{I_S}\right)^3, \tag{11b}$$

which can be used to evaluate all the terms in Eq. (1).

APPENDIX B: HYSTERETIC RESPONSE AND HEATING OF THE NANOBRIDGES

As we discuss in the paper, the resonator exhibits hysteretic response to magnetic flux when the input power is relatively low. Such a behavior occurs, as can be seen from Eq. (7) above, when the screening parameter β_L is sufficiently large to give rise to metastability in the dimensionless potential u. A fitting of the model to the experimental data shown in Fig. 3(a) of the paper yields a value of $\beta_L=7.4$. Another example of hysteretic response is shown in Fig. 6 below that shows data taken with another sample, which was fabricated using the same process that is described in the first section. The larger critical current in that sample yields a larger value of the screening parameter $\beta_L=20$.

As is mentioned in the paper, as the input power is increased the response becomes nonhysteretic. The gradual transition between the hysteretic region to the nonhysteretic one is seen in Fig. 7 below, which shows the difference in the measured resonance frequency of the first mode obtained from increased flux sweep ($f_{1\ inc}$) and decreased flux sweep ($f_{1\ dec}$) at different input powers. Dark blue in the color map corresponds to no difference, namely to monostable regions, whereas in the red regions, where a large difference is observed, the system is bistable. As can be clearly seen from the figure, the bistable regions shrink as the input power is increased. The experimental results suggest that the critical current of the nanobridges drops as the input power is increased, and consequently the response becomes nonhysteretic due to the resultant smaller value of the screening parameter β_L. We hypothesize that the drop in the critical current occurs due to heating of the nanobridges by the input power.

To estimate the effect of heating, we assume the case where the substrate is isothermal and that the heat is mainly dissipated down into the substrate rather than along the film.[46] Moreover, we assume that most of the externally injected power into the resonator is dissipated near the nanobridges, where, the current density obtains its largest value. By estimating the heat transfer coefficient per unit area between each nanobridge and the substrate beneath it (100 nm SiN on top of high-resistivity Si) to be $\kappa \simeq 1$ W cm^{-2} K^{-1} (Ref. 47 and 48) and the area of the nanobridge to be $A \simeq (50$ nm$)^2$ one finds that the expected temperature rise for $P_{in}=-70$ dBm is $\Delta T = P_{in}/A\kappa \simeq 4$ K.

Since heating is produced by AC current flowing through the nanobridges, it is important to estimate also the thermal

rate, which characterizes the inverse of the typical time scale of thermalization, and is given by $\gamma_T = A\kappa/C$, where the heat capacity C of the nanobridge is given by $C = C_v A d$, C_v is the heat capacity per unit volume, and d is the thickness of the superconducting film. Using the estimate C_v

$\simeq 10^{-3}$ J cm^{-3} K^{-1} (Ref. 48) one finds $\gamma_T \simeq 0.1$ GHz. Since the frequency of the AC heating current is 1–2 orders of magnitude higher, we conclude that to a good approximation the temperature of the nanobridges can be considered as stationary in the steady state.

---

[1] W. H. Zurek, Phys. Today **44**, 36 (1991).

[2] N. Imoto, H. A. Haus, and Y. Yamamoto, Phys. Rev. A **32**, 2287 (1985).

[3] B. C. Sanders and G. J. Milburn, Phys. Rev. A **39**, 694 (1989).

[4] W. J. Munro, K. Nemoto, R. G. Beausoleil, and T. P. Spiller, Phys. Rev. A **71**, 033819 (2005).

[5] D. H. Santamore, A. C. Doherty, and M. C. Cross, Phys. Rev. B **70**, 144301 (2004).

[6] E. Buks, E. Segev, S. Zaitsev, B. Abdo, and M. P. Blencowe, EPL **81**, 10001 (2008).

[7] F. Helmer, M. Mariantoni, E. Solano, and F. Marquardt, Phys. Rev. A **79**, 052115 (2009).

[8] E. Buks and B. Yurke, Phys. Rev. A **73**, 023815 (2006).

[9] T. Yamamoto, K. Inomata, M. Watanabe, K. Matsuba, T. Miyazaki, W. D. Oliver, Y. Nakamura, and J. S. Tsai, Appl. Phys. Lett. **93**, 042510 (2008).

[10] M. Sandberg, C. M. Wilson, F. Persson, G. Johansson, V. Shumeiko, P. Delsing, and T. Duty, Appl. Phys. Lett. **92**, 203501 (2008).

[11] A. Palacios-Laloy, F. Nguyen, F. Mallet, P. Bertet, D. Vion, and D. Esteve, J. Low Temp. Phys. **151**, 1034 (2008).

[12] D. I. Schuster, A. Wallraff, A. Blais, L. Frunzio, R.-S. Huang, J. Majer, S. M. Girvin, and R. J. Schoelkopf, Phys. Rev. Lett. **94**, 123602 (2005).

[13] D. Schuster, A. Houck, J. Schreier, A. Wallraff, J. Gambetta, A. Blais, L. Frunzio, B. Johnson, M. Devoret, S. Girvin, and R. Schoelkopf, Nature (London) **445**, 515 (2007).

[14] S. Gleyzes, S. Kuhr, C. Guerlin, J. Bernu, S. Deleglise, U. Hoff, M. Brune, J. Raimond, and S. Haroche, Nature (London) **446**, 297 (2007).

[15] T. D. Clark, R. J. Prance, R. Whiteman, H. Prance, M. J. Everitt, A. R. Bulsara, and J. F. Ralph, J. Appl. Phys. **90**, 3042 (2001).

[16] P. D. Nation, M. P. Blencowe, and E. Buks, Phys. Rev. B **78**, 104516 (2008).

[17] K. K. Likharev, Rev. Mod. Phys. **51**, 101 (1979).

[18] A. G. P. Troeman S. H. W. van der Ploeg, E. Il'Ichev, H.-G. Meyer, A. A. Golubov, M. Y. Kupriyanov, and H. Hilgenkamp, Phys. Rev. B **77**, 024509 (2008).

[19] S. K. H. Lam and D. L. Tilbrook, Appl. Phys. Lett. **82**, 1078 (2003).

[20] G. J. Podd, G. D. Hutchinson, D. A. Williams, and D. G. Hasko, Phys. Rev. B **75**, 134501 (2007).

[21] L. Hao, J. C. Macfarlane, J. C. Gallop, D. Cox, J. Beyer, D. Drung, and T. Schurig, Appl. Phys. Lett. **92**, 192507 (2008).

[22] L. Hao, J. C. Macfarlane, J. C. Gallop, D. Cox, P. Joseph-Franks, D. Hutson, J. Chen, and S. K. H. Lam, IEEE Trans. Instrum. Meas. **56**, 392 (2007).

[23] C. Bell, G. Burnell, D.-J. Kang, R. H. Hadfield, M. J. Kappers, and M. G. Blamire, Nanotechnology **14**, 630 (2003).

[24] A. Datesman, J. Schultz, A. Lichtenberger, D. Golish, C. Walker, and J. Kooi, IEEE Trans. Appl. Supercond. **15**, 928 (2005).

[25] A. Troeman, H. Derking, B. Borger, J. Pleikies, D. Veldhuis, and H. Hilgenkamp, Nano Lett. **7**, 2152 (2007).

[26] A. Datesman, J. Schultz, T. Cecil, C. Lyons, and A. Lichtenberger, IEEE Trans. Appl. Supercond. **15**, 3524 (2005).

[27] B. Yurke and E. Buks, J. Lightwave Technol. **24**, 5054 (2006).

[28] B. Abdo, O. Suchoi, E. Segev, O. Shtempluck, M. Blencowe, and E. Buks, EPL **85**, 68001 (2009).

[29] Y. Levinson, EPL **39**, 299 (1997).

[30] E. Buks, S. Zaitsev, E. Segev, B. Abdo, and M. P. Blencowe, Phys. Rev. E **76**, 026217 (2007).

[31] M. P. Blencowe and E. Buks, Phys. Rev. B **76**, 014511 (2007).

[32] C. Granata, E. Esposito, A. Vettoliere, L. Petti, and M. Russo, Nanotechnology **19**, 275501 (2008).

[33] K. Hasselbach, D. Mailly, and J. Kirtley, J. Appl. Phys. **91**, 4432 (2002).

[34] K. Hasselbach, C. Veauvy, and D. Mailly, Physica C **332**, 140 (2000).

[35] A. Baratoff, J. A. Blackburn, and B. B. Schwartz, Phys. Rev. Lett. **25**, 1096 (1970).

[36] K. K. Likharev and L. A. Yakobson, Sov. Phys. Tech. Phys. **20**, 950 (1975).

[37] A. Gumann, T. Dahm, and N. Schopohl, Phys. Rev. B **76**, 064529 (2007).

[38] A. V. Pronin, M. Dressel, A. Pimenov, A. Loidl, I. V. Roshchin, and L. H. Greene, Phys. Rev. B **57**, 14416 (1998).

[39] B. W. Maxfield and W. L. McLean, Phys. Rev. **139**, A1515 (1965).

[40] A. A. Golubov, M. Y. Kupriyanov, and E. Il'ichev, Rev. Mod. Phys. **76**, 411 (2004).

[41] K. Mitra, F. W. Strauch, C. J. Lobb, J. R. Anderson, F. C. Wellstood, and E. Tiesinga, Phys. Rev. B **77**, 214512 (2008).

[42] J. F. Ralph, T. D. Clark, R. J. Prance, H. Prance, and J. Diggins, J. Phys.: Condens. Matter **8**, 10753 (1996).

[43] R. G. Littlejohn and W. G. Flynn, Phys. Rev. A **44**, 5239 (1991).

[44] G. Panati, H. Spohn, and S. Teufel, Phys. Rev. Lett. **88**, 250405 (2002).

[45] C. D. Tesche and J. Clarke, J. Low Temp. Phys. **29**, 301 (1977).

[46] M. W. Johnson, A. M. Herr, and A. M. Kadin, J. Appl. Phys. **79**, 7069 (1996).

[47] E. Monticone, V. Lacquaniti, R. Steni, M. Rajteri, M. Rastello, and L. Parlato, IEEE Trans. Appl. Supercond. **9**, 3866 (1999).

[48] K. Weiser, U. Strom, S. A. Wolf, and D. U. Gubser, J. Appl. Phys. **52**, 4888 (1981).